SANDIA REPORT
SAND2017-5358
Unlimited Release
Printed May 2017

Corrosion Monitors for Embedded Evaluation

Alex L. Robinson, Kent B. Pfeifer, Adrian L. Casias, Stephen W. Howell, N. Robert Sorensen, Nancy A. Missert

Prepared by
Sandia National Laboratories
Albuquerque, New Mexico 87185 and Livermore, California 94550

Sandia National Laboratories is a multimission laboratory managed and operated by National Technology & Engineering Solutions of Sandia, LLC., a wholly owned subsidiary of Honeywell International, Inc., for the U.S. Department of Energy's National Nuclear Security Administration under contract DE-NA0003525.

Issued by Sandia National Laboratories, operated for the United States Department of Energy by National Technology and Engineering Solutions of Sandia, LLC.

Available to DOE and DOE contractors from
U.S. Department of Energy
Office of Scientific and Technical Information
P.O. Box 62
Oak Ridge, TN 37831

Telephone: (865) 576-8401
Facsimile: (865) 576-5728
E-Mail: reports@osti.gov
Online ordering: http://www.osti.gov/scitech

Available to the public from
U.S. Department of Commerce
National Technical Information Service
5301 Shawnee Rd
Alexandria, VA 22312

Telephone: (800) 553-6847
Facsimile: (703) 605-6900
E-Mail: orders@ntis.gov
Online order: http://www.ntis.gov/search

SAND2017-5358
Printed May 2017
Unlimited Release

Corrosion Monitors for Embedded Evaluation

Alex L Robinson
Special Use Hi-Reliability Capacitors Department

Kent B Pfeifer
Nano and Micro Sensors Department

Adrian L Casias
Microsystem Packaging & Polymer Processing Department

Stephen W Howell
Applied Photonic Microsystems Department

Neil R Sorensen
Materials Reliability Department

Nancy A Missert
Nanoscale Sciences Department Department

Sandia National Laboratories
P.O. Box 5800
Albuquerque, New Mexico 87185-MS0525

Abstract

We have developed and characterized novel in-situ corrosion sensors to monitor and quantify the corrosive potential and history of localized environments. Embedded corrosion sensors can provide information to aid health assessments of internal electrical components including connectors, microelectronics, wires, and other susceptible parts. When combined with other data (e.g. temperature and humidity), theory, and computational simulation, the reliability of monitored systems can be predicted with higher fidelity.

ACKNOWLEDGMENTS

The authors would like thank Anthony J. (TJ) Ross III* for preparation of substrates and sensor fabrication; Catherine E. Sobczak for bond pad processing and handling; Jonathon M. Rivera for aluminum sensor fabrication and testing; Arthur N. Rumpf for PC board fabrication; Tom A. Hill for providing silicon wafers with deposited bond pads; Samuel J Lucero* for support with corrosive environment testing, Gerald M. Boyd for RC circuit simulations; George Laguna* for conversations regarding surface capacitors; and Diane E. Peebles, Richard W. Cernosek*, and Jeff W. Braithwaite* for programmatic support.

*Retired or no longer active at Sandia National Laboratories.

FOREWORD

The research and results reported here were completed in September 2009. The final programmatic report has been edited for release in this SAND Report. Minor updates not included in the final report are found herein.

CONTENTS

FIGURES

TABLES

NOMENCLATURE

°C	degrees Celsius
Å	Angstrom
A/D	analog to digital
AMPL	Advanced Manufacturing Processes Laboratory
ASIC	application specific integrated circuit
C	capacitance
CMOS	complementary metal-oxide semiconductor
COTS	commercial off-the-shelf
DOE	Department of Energy
IC	integrated circuit
IDE	interdigitated electrode
IDT	interdigitated transducer
kΩ	kilo-ohm
μA	micro-amp
MESA	Microsystems and Engineering Sciences Applications
μm	micron
mm	millimeter
mTorr	milli-torr
MOS	metal-oxide semiconductor
MΩ	mega-ohm
NEMA	National Electrical Manufacturers Association
PC	personal computer
pf	pico-farad
PIC	Peripheral Interface Controller
ppb	parts per billion
RPM	revolutions per minute
RH	relative humidity
sccm	standard cubic centimeters per minute
UART	universal asynchronous receiver/transmitter
USB	universal serial bus
UV	ultra-violet
V	volts
Vcc	voltage at the common collector
Ω	ohm
W	watt

1. INTRODUCTION

Atmospheric corrosion is an age-related degradation process with a high likelihood of occurrence and the potential to adversely impact the performance of electrical devices [1-3]. In-situ corrosion sensors have been investigated to monitor and quantify the corrosive potential of atmospheres in controlled environments. Embedded corrosion sensors have the potential to provide information for assessing the health of incorporated electrical components including connectors, microelectronics, wires, and other susceptible parts. Combined with other sensor data (e.g. temperature, humidity), theory, and computational simulation, the reliability of monitored systems can be determined with higher fidelity.

Two materials commonly found to corrode in electrical devices are copper and aluminum. Both are susceptible to corrosion in the presence of moisture and other chemicals. For copper, sulfur-bearing compounds spontaneously decompose to form copper sulfide (Figure 1). Spontaneously formed copper ions are highly mobile, and the process continues to penetrate deeper into the copper substrate [1,2]. Sulfidation can cause an electrical open when copper sulfide forms between two elements of a switch or connector. The common household light switch is designed to wipe clear the copper contact elements upon actuation to ensure continuity. This cannot be done reliably in a make-once connection or switch that is unattended over many years. Copper (II) sulfide is also a semi-conductor, which may cause electrical shorting in other situations.

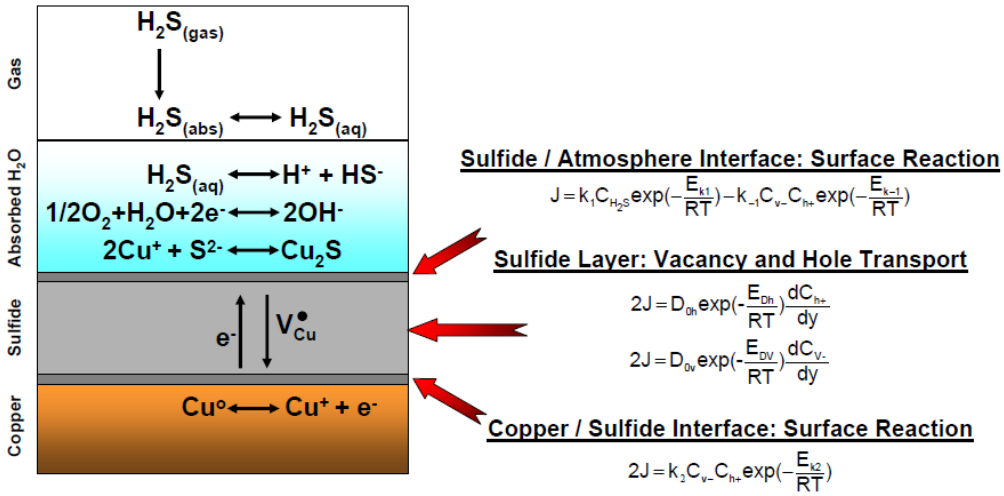

Figure 1. Sulfidation of copper in the presence of hydrogen sulfide and moisture.

Aluminum and aluminum/copper alloys are susceptible to corrosion in the presence of moisture and chloride ions. Corrosion tends to manifest as localized pitting and filamentary voids [3]. For modern microelectronics and MEMS devices, this can lead to failure in short periods of time. Galvanic coupling, for instance with gold wire bonds connecting the device to the carrier substrate, can accelerate corrosion at locations proximate to the coupling.

Corrosion of these materials has been studied over the years using bare substrates and witness plates. In more recent years researchers have used photolithographically defined structures on relatively large substrates [4]. The work presented here re-engineers this concept into small sensors to enable direct incorporation onto electrical circuit boards in locations where many of these issues arise. Microfabrication leads to smaller, lighter, more reproducible, stable, and inexpensive devices.

2. APPROACH

Sensors. Three different types of sensors were fabricated for monitoring corrosive environments. The first consists of thin films of copper or aluminum/copper alloys in a serpentine spiral design, 18.3 mm in length calculated along the middle of the path. As corrosion progresses, resistance climbs and eventually reaches a value determined by the thin, metal adhesion layer. The spirals were photolithographically defined on substrates of amorphous alumina and sapphire, respectively. Sputtered copper thicknesses were 500, 1000, and 2000 Angstroms (Å), with widths of 50, 100, and 200 microns. Aluminum widths were the same, and thickness was typically 2000 Å, deposited by e-beam chemical vapor deposition (CVD). In these devices, the percentage of copper co-deposited ranged from 0 to 3.5%. Various annealing temperatures of the alloys added another parameter for testing. After deposition, the 0.030" thick substrates were diced with a wafer saw at Sandia's AMPL facility to a standard 1808 size (0.180" L x 0.080" W). This is a common size for surface mount electrical components on circuit boards. The ends and vertical edges were then sputter-coated with 200Å titanium (adhesion layer), 5000 Å nickel, and 2000 Å gold through a shadow mask to form solder pads separated by the resistive film. A representative design is shown schematically in Figure 2, and actual devices are shown in Figure 3 and Figure 4. More detailed process steps are provided in Appendix A. Once solder pads were added, these sensors were soldered to printed circuit boards designed to directly measure resistance by a low-power analog-to-digital circuit. Gold reference sensors were made alongside the copper sensors with a thickness of 2000 Å. These served as reference devices during experiments.

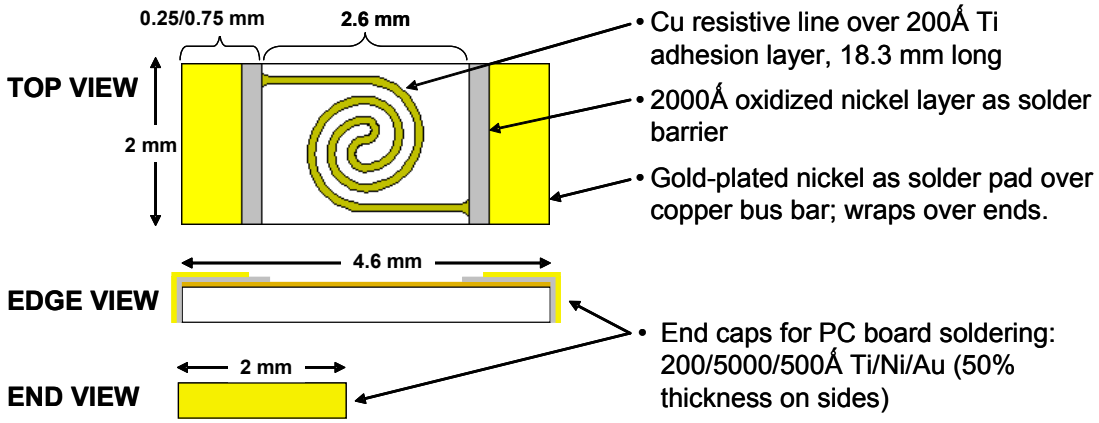

Figure 2. Schematic of resistive serpentine microfabricated corrosion sensor. Edge view shows various layers in the metal stack. Capacitive IDE sensors were co-fabricated from the same mask.

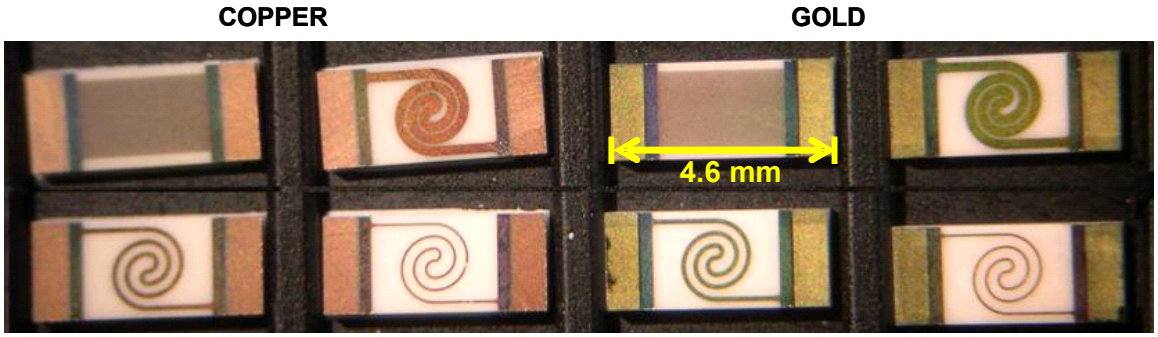

Figure 3. Microfabricated copper corrosion sensors (left four) and gold reference devices (right four). The copper sensors shown here have the nickel solder barrier strip, but the Ni/Au solder layer was not yet added. Clockwise from the upper left for each set of sensors are 1) capacitive IDE sensor, 2) 200 μm wide, 3) 50μm wide, and 4) 100 μm wide resistive sensors. Aluminum sensors not shown.

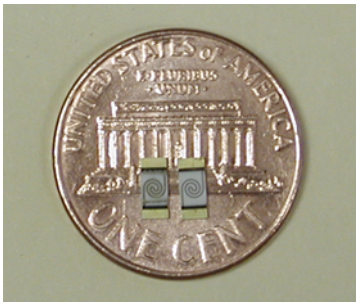

Figure 4. Two sensors side-by-side on a penny for size reference.

The second sensor type was co-fabricated with the resistive sensors and has the same size, solder pads, metals, and film thicknesses. However, the sensing pattern was a pair of interdigitated electrodes (IDEs), shown in Figure 3, upper left. This pattern behaves as a capacitor when charge is applied or allowed to drain. With 50 finger pairs ~2.5 mm long, capacitance of 14.7 +/-0.2 pico-farads (pF) was obtained. This compared favorably to the calculated value of 11 pF. When paired with a high value resistor (e.g. 1 MOhm), this sensor can be read as an RC circuit by monitoring its charge/discharge time constant (Figure 5). The circuit was charged by a digital line in, using very low power. When a voltage comparator senses that the circuit voltage has risen to approximately 70% of Vcc, it toggled an interrupt to mark the elapsed charge time, per the number of elapsed oscillator clock cycles since the digital line was energized. A simulation of the behavior is shown in Figure 6. The sensor's time constant changes progressively with consumption of the metal layer. It was expected that corrosion of the copper or aluminum IDEs would be observed as a loss of capacitance as the copper conductor corroded, although a different effect dominated. This is described later.

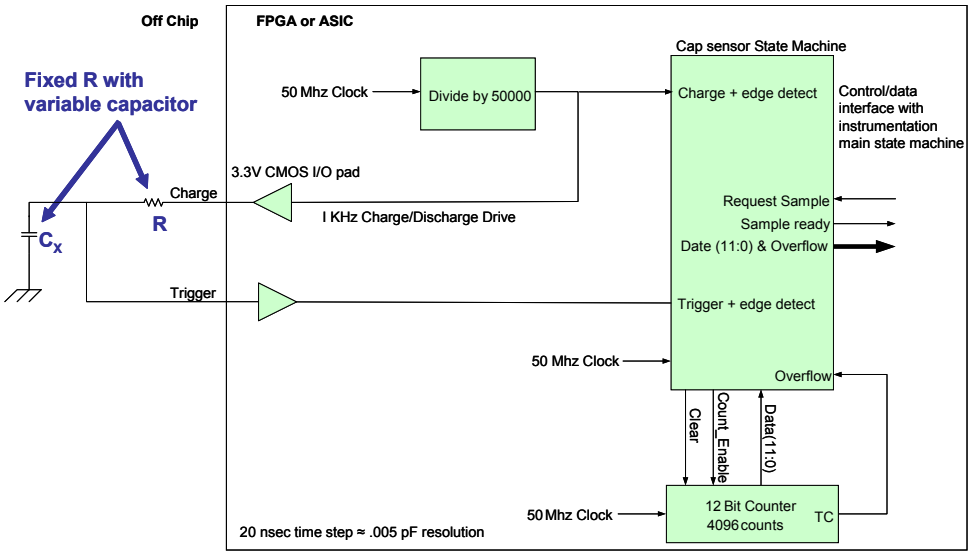

Figure 5. Schematic of RC time constant measurement circuit for measuring changes in the capacitive sensors (courtesy of Gerald Boyd, Dept 5355).
The external RC circuit (capacitive sensor) is charged by the microprocessor, which also calculates the RC time constant from the number of clock cycles required to reach 1/2Vcc.

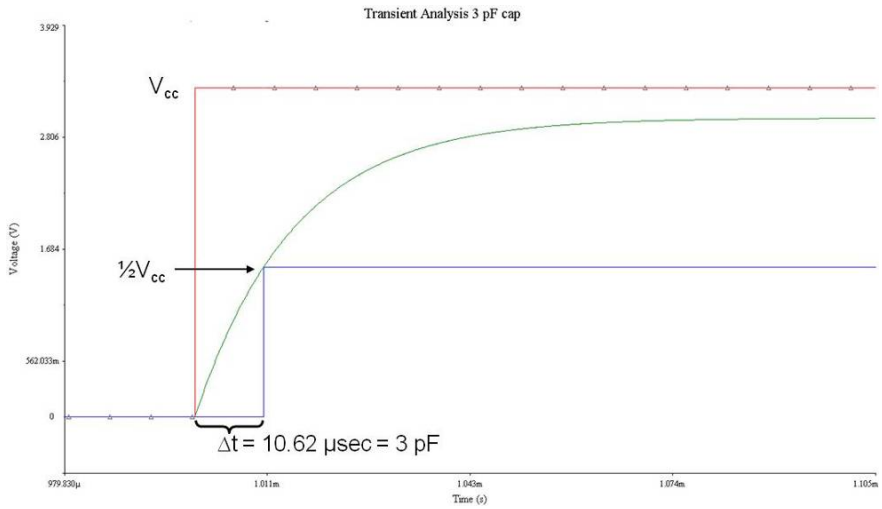

Figure 6. Simulation of RC sensor charging (courtesy of Gerald Boyd, Dept 5355).

The third sensor type was designed to monitor integrity of wire bonds on aluminum bond pads (Figure 7). These sensors started in Sandia's MESA facility using a top-layer photolithography mask for semi-conductor microelectronic devices on 6" diameter silicon wafers. The pads are typically used for wire bonding devices to carrier packages before polymer encapsulation. They are identical to those in actual semi-conductor devices in metal composition, thickness, adhesion layer, dielectric, pitch, and processing. Composition is typically aluminum with 0.5% copper. The only significant difference was that our sensor pads were not electrically connected to semi-conductor circuits within the silicon layer and lacked the corresponding vias.

The silicon wafers were then diced to make hundreds of 1808 sized devices, followed by top and edge metallized to form solder pads like the other two sensor types. Wire bonding was then performed to jumper select solder pads together making multiple ball-and-stitch connections across the middle. One mil (0.001") diameter gold wire was used, which is typical of MESA

microelectronics. Increasing the number of wire bonds increases the likelihood of a single failure causing an electrical open. The micro-scale crevices that form at the bonds serve as sinks where moisture condenses spontaneously or migrates from across surfaces to form liquid water. A magnified image of a stitch bond is shown in Figure 8.

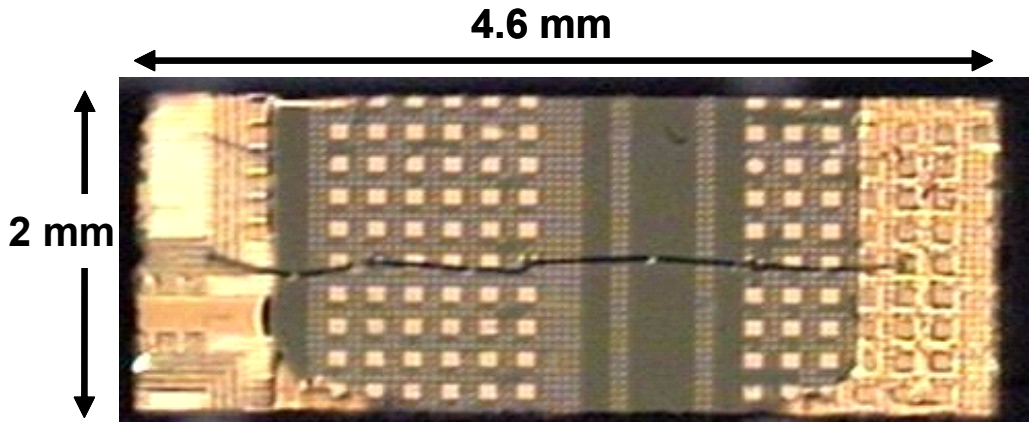

Figure 7. Bond pad sensor with nickel/gold solder pads and a 0.001" gold wire jumpered across multiple wire-bond pads from end to end.
Bond pads were aluminum with 0.5% copper from the MESA Fab.

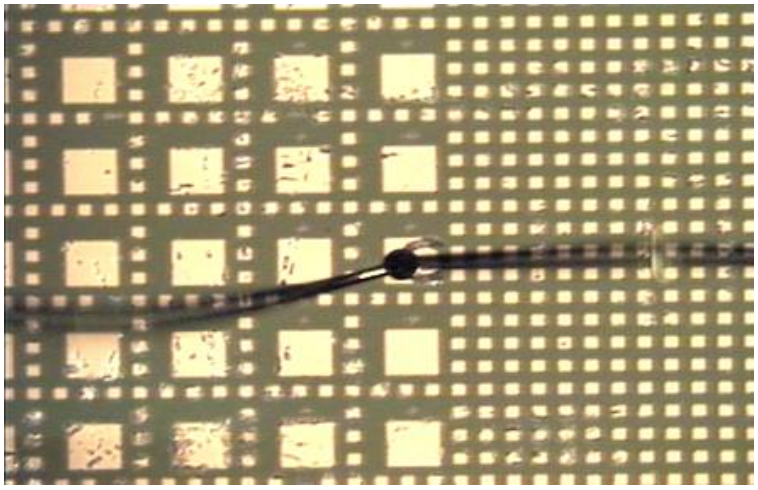

Figure 8. Microscope image of 0.001" gold wire stitch bond on 100μm x 100μm bond pad.

While not attained at this writing, the next step planned for these sensors is ion implantation of chloride into the aluminum/copper pads to seed corrosion. Implanted concentrations can be above and at various steps below the threshold value known to induce spontaneous corrosion. Wire bonding before and after the implant step will need to be evaluated to determine the best method for obtaining a robust early warning microelectronics failure sensor. With successive circuit openings of the progressively seeded sensors, a time-to-failure of the unseeded device (and nearby electronics) will be predictable.

PC Test Boards. Multiple sets of resistive and capacitive PC board-mountable corrosion sensors were fabricated. To facilitate testing and emulate an actual system, two circuit boards were designed based on a PIC 18F4550 microcontroller, fabricated, and populated with sensors (Figure 9). Communication to a PC was via a USB connection programmed to mimic a universal

asynchronous receiver/transmitter (UART). The PICs were programmed using C language from Customer Computer Services, Inc. (CCS). The architecture of both boards was similar except for the measurement sections. For measurement of the resistance devices, a switchable constant-current source was used to produce a voltage drop across the resistors that was then measured using an on-board 10-bit analog-to-digital (A/D) converter on the microcontroller. Multiplexers allowed serial measurement of 12 sensors plus a reference. For measurement of capacitive sensors, each was configured in an RC circuit with a fixed 2.2 MΩ resistor. As the applied voltage switched from ground to V_{cc}, the voltage at the capacitive sensor rose until a Schmitt trigger changed logic state at slightly over $1/2V_{cc}$. The microcontroller measured the rise-time using the board's master oscillator. Capacitance was then calculated using the RC time constant and number of elapsed clock cycles. After the Schmitt trigger state changed, voltage was removed from the circuit and voltage decayed back to zero. Twelve capacitive sensors, a reference capacitor, and four wire-bond sensors could be monitored directly from the PIC on this board. In addition to corrosion sensors, both boards also contained a temperature compensated relative humidity sensor and a temperature sensor. Boards were coated with protective conformal coating before addition of the corrosion sensors to protect the other components and surfaces from corrosion. Additional details are given in Appendix B.

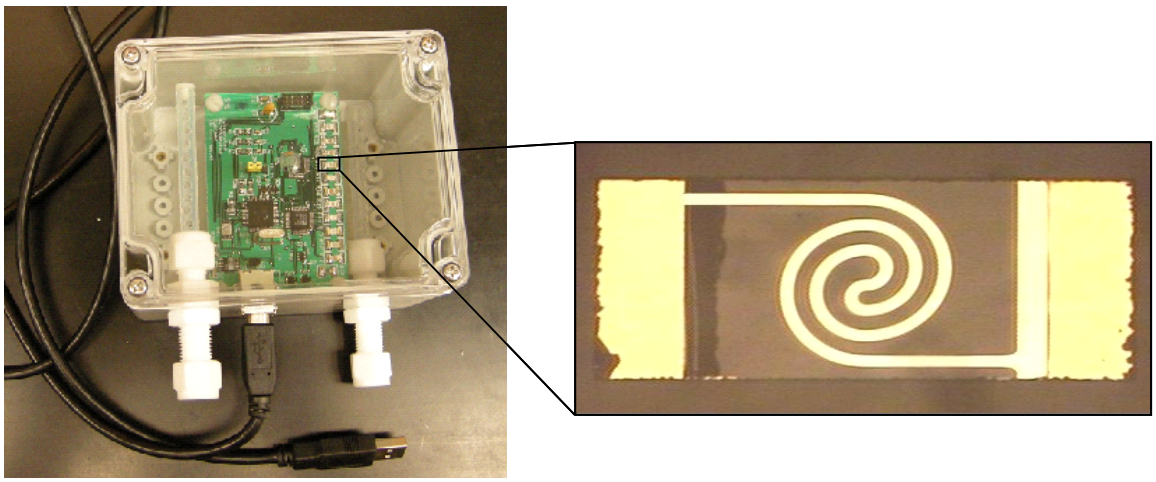

Figure 9. Resistive sensor PC test board protected with conformal coating and placed in 4.5" x 3.5" x 3.2" NEMA box.
Teflon gas ports, gas diffusing tubes, and USB cable are visible.

Test Fixtures and Vapor Generator. To test the sensors in corrosive environments, test cells were constructed from polycarbonate NEMA enclosures (Figure 9). These were each fitted with two 1/4" Teflon bulkheads (Swagelok) connected to internal perforated tubing to facilitate even distribution and venting of test gases with no direct impingement of flow on the sensors. PC boards were fixed to the test cell base using polypropylene stand-offs and screws. After sealing gaps, such as around the USB port, a text cell was connected to a vapor mixing apparatus to create a well-controlled corrosive gas stream.

The gas stream was created by mixing humid nitrogen with a sulfur gas. In a large oven set to 30°C, nitrogen gas flowed through a fritted bubbler containing deionized water. A second dry nitrogen stream flowed over a diffusion tube containing liquid hydrogen sulfide. The two streams were mixed to generate an environment in Table 1, which then flowed through the NEMA box

containing the sensor suite under test. Data was collected in real-time at 10 minute intervals over multiple days using a custom LabVIEW program to communicate with the PC boards.

Table 1. Corrosion test environments for challenging sensors.

	Environment 1	**Environment 2**
Temperature:	30°C	30°C
Relative Humidity:	70%	70%
Flow rate:	100 sccm	1000 sccm
H_2S Concentration:	10 ppb	100 ppb
Acceleration Factor:	250	2500

A standard Class II environment contains 10 ppb H_2S, 200 ppb NO_2, and 10 ppb Cl_2 at 70% RH and 30 °C) and creates a corrosion acceleration factor of approximately 250 relative to typical indoor conditions. At this rate, two weeks of vapor exposure approximates 9.5 years. As our vapor streams did not contain nitrogen dioxide or chlorine gas, the environment was less complex and the acceleration factor could not be directly compared, but corrosion still proceeded at a significant rate for the copper corrosion sensors. The rate of sulfidation is linear with hydrogen sulfide concentration, so our Environment 2 presented a ten-fold increase in corrosive potential over Enivironment 1.

3. RESULTS

Copper Resistive Sensors. Testing began with the copper sensors, which consisted of the parameters shown in

Table 2. The sensors had been kept in a dry nitrogen environment as much as possible between and after processing steps. This should keep oxide layers thin, maximizing initial conductivity and minimizing the induction period when sulfur competes to remove the oxygen barrier. According to the fixed resistor the time-based conversion creates an offset of 4.9 Ohms, which should be constant on all channels. Some sensors showed a much greater change after soldering, possibly from breaking through surface contamination. Changes of less than 5 Ohms can be accounted for as a slight increase in resistance from accelerating oxidation of the copper conductor during the high temperature soldering. Most sensors measured within 50% of their theoretical initial values, with a few that measured too low (R15, R16*, R22 and R23). Low measurements of the 200 μm wide sensors was due to shorter than calculated conductance paths along the very wide serpentines (see Figure 3).

Table 2. Metal parameters of resistive sensors on first PC test board.
All have 200Å thick titanium adhesion layer under the copper layer.

Channel	Material	Width, microns	R before soldering	R from PC test board	Expected resistance
R23	Cu 500Å	50	303 Ω	31.9 Ω	120.9 Ω
R22	Cu 500Å	100	207 Ω	25.2 Ω	60.4 Ω
R21	Cu 500Å	200	52.0 Ω	49.4 Ω	30.2 Ω
R20	Cu 1000Å	200	21.7 Ω	17.0 Ω	15.2 Ω
R18	Cu 1000Å	100	34.7 Ω	30.0 Ω	30.5 Ω
R17	Cu 1000Å	50	74.4 Ω	72.2 Ω	60.9 Ω
R16*	Cu 2000Å	200	8.3 Ω	1.45 Ω	7.6 Ω
R15	Cu 2000Å	100	17.2 Ω	10.65 Ω	15.3 Ω
R14	Cu 2000Å	50	35.5 Ω	29.5 Ω	30.6 Ω
R13	Cu 500Å	50	1558 Ω	-	120.9 Ω
R12	Cu 500Å	100	944 Ω	-	60.4 Ω
R11	Cu 500Å	200	53.0 Ω	46.9 Ω	30.2 Ω
R10	Fixed Resistor	-	100.0 Ω	94.9 Ω	100.0 Ω

The vapor generator system was set up to generate the conditions of Environment 1 in Table 1. Once conditions stabilized, the NEMA box was attached and data acquisition began immediately. When the sensor board was removed after 301 hours, corrosion of the sensors was clearly visible. Figure 10 shows magnified images of a corrosion sensor before soldering to the PC test board, and after exposure to the corrosive environment. The other electronics, protected with conformal coating, showed no noticeable signs of corrosion.

* This sensor had anomalously low resistance measurements throughout experimentation. Some parallel conductive path likely existed.

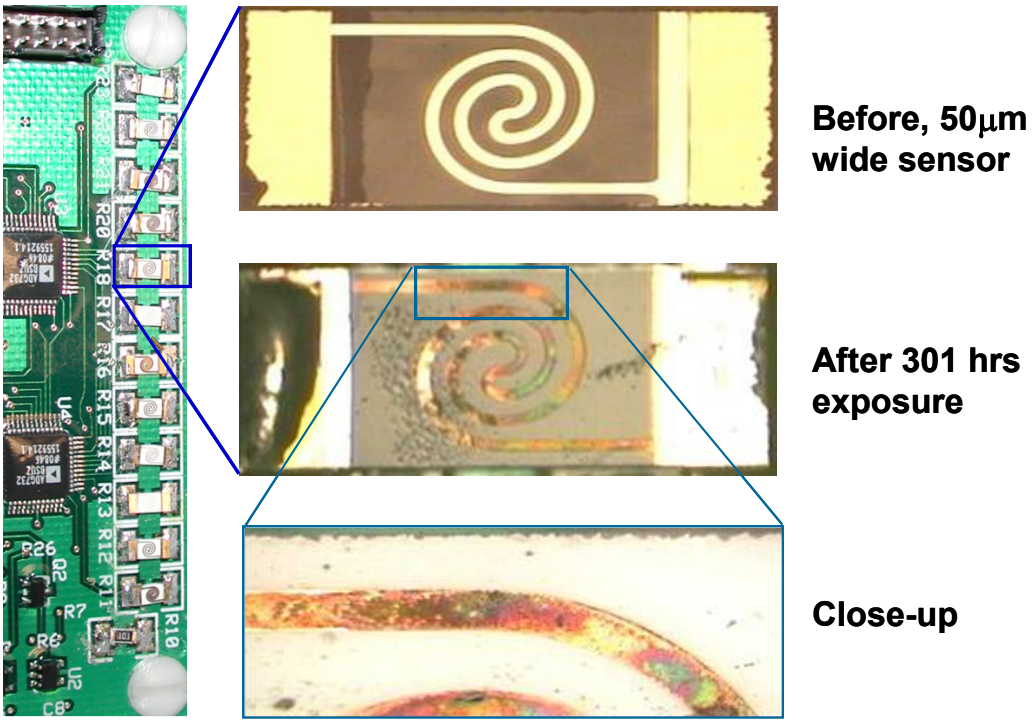

Figure 10. Twelve copper resistive sensors of various widths and thicknesses on PC test board. A 50μm wide sensor is magnified, before soldering and after exposure to Environment 1. It can be seen that corrosion does not occur uniformly across the copper surface.

Figure 11 shows the response of six sensors coated with 500 Å thick copper to to 301 hours of testing. This time approximates 8.6 years in a low humidity, static, but complex environment. It appears some of the sensors started corroding before data acquisition began. Near the ends of their lifetimes, sensor pairs produced nearly overlapping readings as they asymptotically approached their final values. Initial results indicate good reproducibility and correlation between the 50 and 100 μm wide sensors. The 200 μm wide sensors are more likely to stray from predicted behavior, but may be more robust to initial bias from premature corrosion.

Once all the copper has been converted to non-conductive copper sulfide, the residual conductivity was due to the titanium adhesion layer. If an assumption is made that this process is 100% complete at 300 hours, then the final conductivity of the 50 and 100 μm wide sensors indicates a metallic titanium layer of 115 +/-2 Angstroms thick. This is a reasonable value considering part of the titanium layer is consumed in making strong covalent bonds with the alumina interface. Conductivity of the 200 μm wide sensors is greater than 200 Å of titanium would indicate, once again attributed to the very wide serpentine structures short-cutting the linear length at the wide turns.

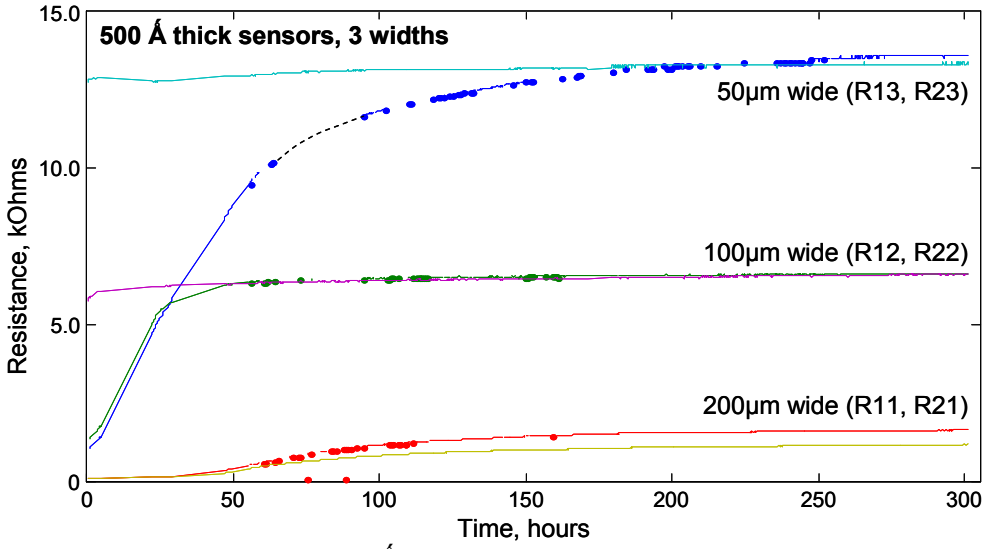

Figure 11. Resistance over time of 500Å thick copper sensors tested in corrosive Environment 1. Some sensors began corroding before data acquisition began. Final values are reproducible, with greater error for the wider trace sensors. Sensors were removed after 301 hours, approximately equivalent to ~8.6 years in a low humidity, complex but static environment.

Figure 12 shows changing resistance with time of three different thickness of the 50 µm wide copper sensors. Corrosion of the thinnest deposition (500 Å) was well under way when data acquisition began. Dashed lines mark the points where resistance increased 50% from baseline to the values at 301 hours. These happen to correspond well with their inflection points as they transition from linear Phase I corrosion to depletion of the copper layer and corresponding non-linear effects. Given enough time, all three sensors should approach the same final value determined by just the titanium adhesion layer.

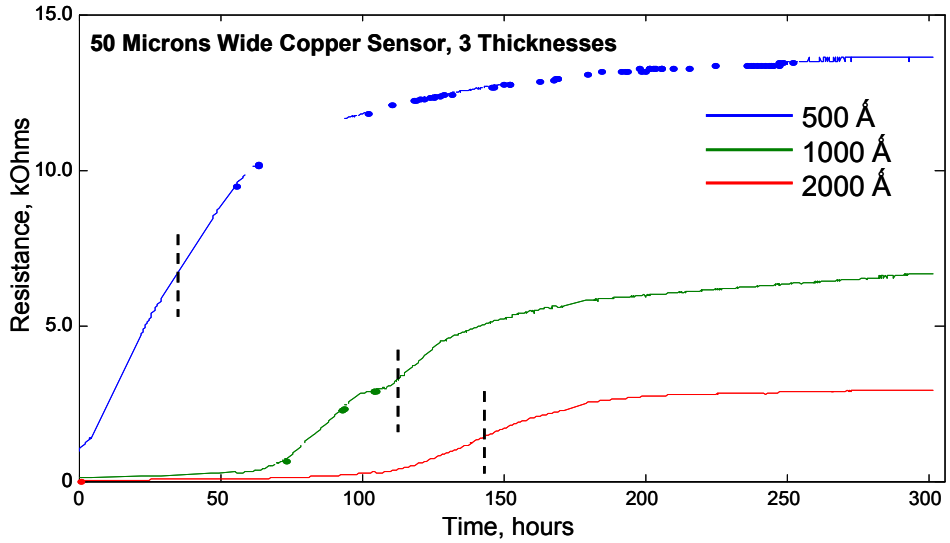

Figure 12. Resistance as a function of time for three 50 micron wide resistive sensors tested in corrosion Environment 1.
Some data points for the 500 Å thick sensor were lost. Dashed vertical lines indicate point where ΔR/R equals 50%.

Figure 13 (left) shows the same data overlapped through auto-scaling and shifting along the time axis. This removes effects of induction delays and demonstrates the linear time dependence of corrosion under Environment 1 conditions for the 3 thicknesses examined. Figure 13 (right) shows the raw data converted to percent copper thickness. Copper depletion is linear with time as a function of percent thickness with a slope of 0.75% per hour. This is non-linear with absolute copper thickness. Corrosion rates slow when copper is nearly depleted in the transition region from copper to titanium. Titanium likely has a stabilizing effect in the intermetallic region that is eventually overcome by the oxidation potential of the sulfur. These results show that even the thickest copper sensor corroded according to Phase I kinetics. Thicker sensors that transition to Phase II corrosion, where the corrosion rate is diffusion limited by copper ion mobility rather hydrogen sulfide concentration, will enable longer sensing lifetimes. Transition to Phase II has been shown to occur at thicknesses greater than 2500 Å [5,6].

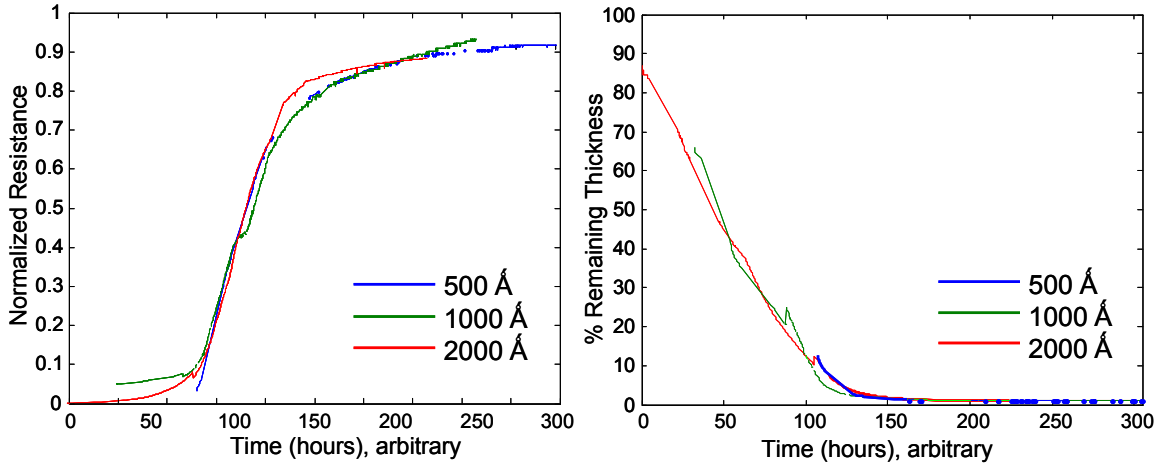

Figure 13. Normalized resistance for three different thicknesses of 50µm wide copper sensors (left), and same data showing remaining copper thickness (right).
Both plots have traces aligned by shifting along the time axis. Thinner sensors had a smaller fraction of their original copper thickness remaining by the beginning of testing.

The data was further analyzed to understand the non-linear rate of loss of copper. Copper thickness was plotted from the resistance data, correcting for the various widths. Results resembled Figure 13 (right), with a linear region for each sensor and a transition to the copper/titanium intermetallic region. The slope of linear region was measured for each sensor. Results are shown in Table 3, and plotted in Figure 14. Rate of loss is first-order with initial copper thickness with a slope of 0.008 Å per hour per Angstrom of initial thickness. Thicker initial copper layers corrode at a faster rate throughout their lifetime. An explanation for this behavior is under investigation. It may be related to a physical phenomenon, such as film stress. Or the interaction zone between copper and sulfur extends beyond the upper-most 2000 Å of thickness. Figure 15 shows that the final sensor resistance after corrosion is complete is inversely proportional to the sensor line width.

Table 3. Rate of copper loss, as calculated from resistance values during corrosion.
Locations with an 'x' were not used in the calculations as these had lost >95% thickness by the first data measurement. R16 had previously been identified as an outlier. Note: the table has been reordered from above to group copper deposition thickness.

Channel	Material, initial thickness	Width, ⍰m	Rate of Cu loss, Å/hr	Mean	St. dev.
R23	Cu 500 Å	50	2.26		
R22	Cu 500 Å	100	x		
R21	Cu 500 Å	200	3.32		
R13	Cu 500 Å	50	x		
R12	Cu 500 Å	100	x		
R11	Cu 500 Å	200	3.58	3.1	0.7
R20	Cu 1000 Å	200	9.87		
R18	Cu 1000 Å	100	7.63		
R17	Cu 1000 Å	50	7.73	8.4	1.3
R16	Cu 2000 Å	200	-		
R15	Cu 2000 Å	100	15.55		
R14	Cu 2000 Å	50	14.53	15.0	0.7

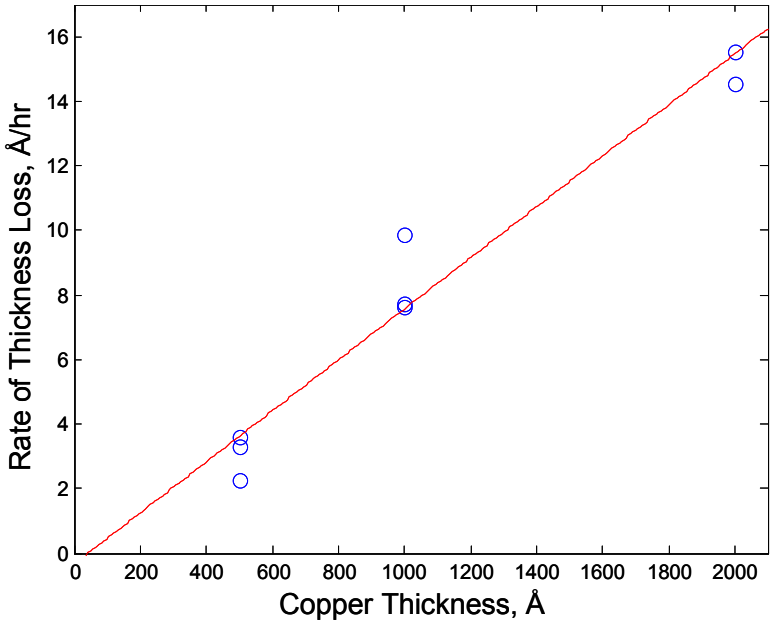

Figure 14. Rate of loss of copper as a function of initial copper thickness.
Loss is first-order with copper thickness.

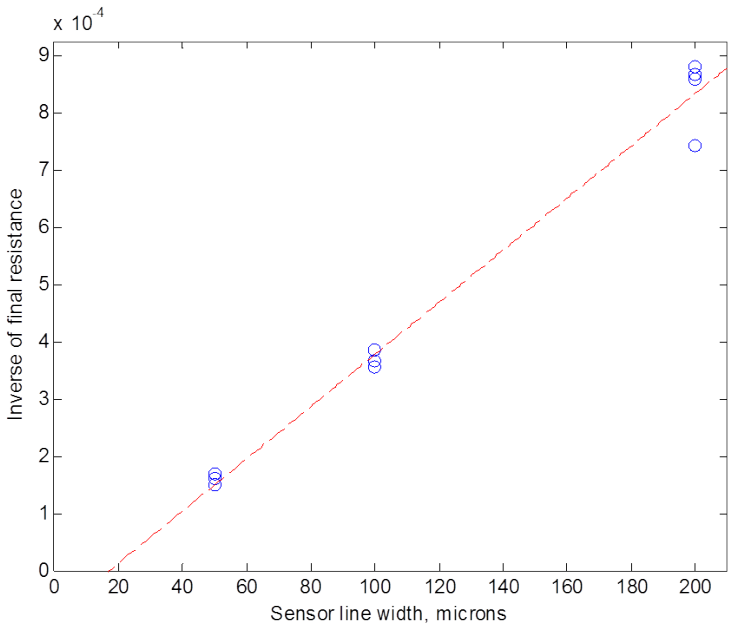

Figure 15. Final sensor resistance after corrosion is complete as a function of sensor line width. Data for 500 Å thick copper sensors is shown, but this result is the same for all thicknesses.

Capacitive Sensors. Next, capacitive sensors were characterized and tested. Capacitance of copper, aluminum, and gold IDE devices were measured by a free-standing capacitance meter. Values measured 14.8 +/-0.3 pF with no correlation to metal thickness or type. For a surface capacitor of this type, capacitance is primarily a function of the metalized footprint and the dielectrics of the substrate and gaseous surroundings (i.e. air). In concept, we initially expected to see a changes in capacitance as copper corroded to copper sulfide, with approximately 33% volumetric expansion and a different dielectric constant. This is shown schematically in Figure 16. A more rigorous understanding of the devices led us to conclude that the capacitance likely had minimal changes during corrosion, and these were eclipsed by other effects, as explained below.

$$V = V_{cc} * (1 - e^{-t/RC})$$

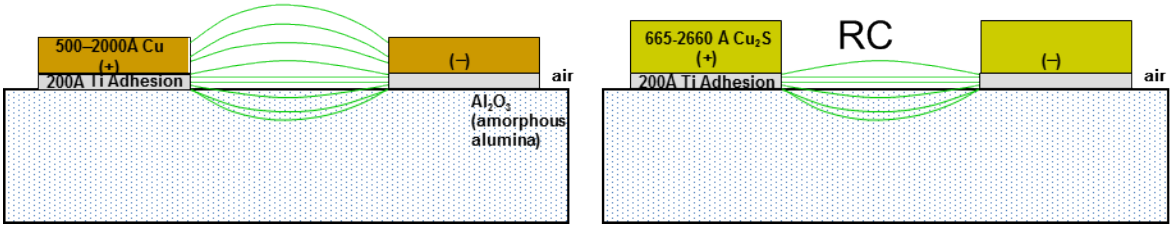

Figure 16. RC time constant of IDE sensor changes with corrosion of copper layer. The change in resistance of the electrode fingers has a much larger effect than the change in capacitance.

A selection of 9 copper capacitive sensors, 2 gold reference devices, and a commercial MOS capacitor were soldered to a capacitive sensor PC test board. Capacitance values calculated from the RC time constants showed an offset of ~5 pF. Other COTS capacitors were tested with the same shift, proving this was an artifact of the timing method with the processor, with a small contribution arising from line inductance. Figure 17 shows experimental data obtained during

exposure to Environment 2 conditions (Table 1) for 100 hours, approximately equivalent to 28.5 years of a low humidity, complex, static environment. Rather than a slow increase or decrease in capacitance, sudden jumps were observed after delays proportional to initial copper thickness. Capacitance values changed from ~20 pF to 385 pF over the course of 10 minutes to 6 hours. The delay was directly proportional to copper thickness (Figure 17), contrary to observations with the resistive sensors. Two of the 9 sensors failed to change for unknown reasons. The COTS capacitor did not change value at all, and the gold devices changed by 0.5 pF when the test environment changed from air to the Environment 2 stream.

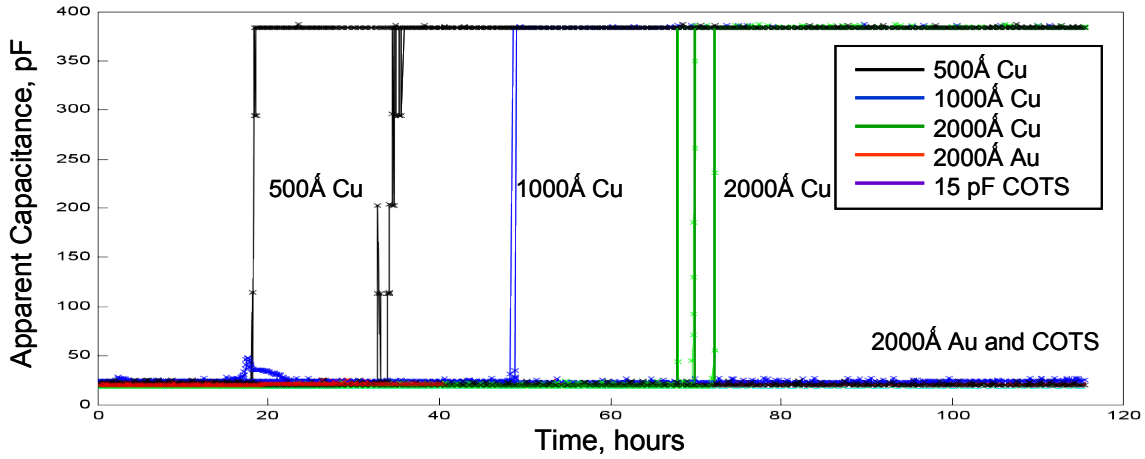

Figure 17. Response of capacitive sensors to Environment 2.
2 hours of N_2; 14.5 hours of room air; 100 of hours of 100 ppb H_2S, 30ºC, and 85% RH. This is approximately equivalent to 28.5 years in a low humidity, complex, static environment.

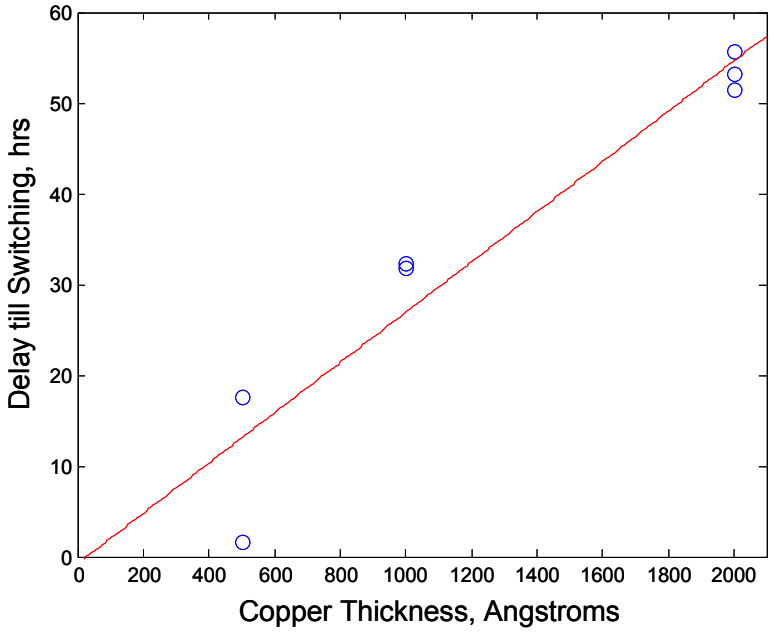

Figure 18. Effect of copper thickness on delay in capacitive sensor switching.

The switch-like behavior of the capacitive sensors as well as the dramatic increase in apparent capacitance led to the conclusion that a different mechanism was responsible for increasing the RC time constant. Further analysis led to several conclusions: 1) the capacitance does not change

significantly as long as there is a metal conductor present, in this case the titanium adhesion layer; 2) the high inherent resistance of the thin titanium layer coupled with loss of copper greatly changes the R contribution of the RC circuit; and 3) photolithographic depositions are highly reproducible from run to run for the titanium layer. Greater variance was seen due to the overlying conductor thicknesses than from the titanium remaining after corrosion. A simplified model of the resulting RC circuit is shown schematically in Figure 18. Using data from the resistive copper sensors, the titanium layer is also likely on the order of 115 Å thick. For a single interdigitated finger 8 μm wide x 2.5 mm long, the calculated resistance is 11.4 kOhms, or double this for a finger pair.

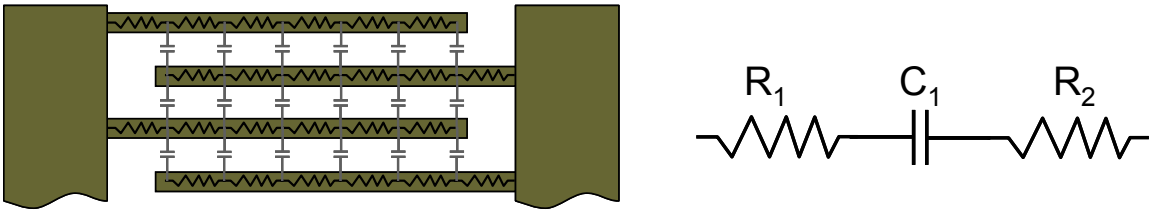

Figure 19. Schematic of interdigitated electrode surface capacitor with resistive fingers. R1 + R2 is on the order of 23 kOhms for each finger pair.

4. NEW CAPACITIVE SENSOR DESIGN

After the unexpected switch-like responses of the original capacitive sensors, a new design was conceived. Figure 20 shows a cross-section schematic of metallized structures opposing each other across an air gap. This configuration forces field lines to pass through the full structure as the copper metal converts to copper sulfide. As the composition of dielectric material changes from just air to include cuprous sulfide, the effective capacitance C_{eq} of the circuit increases until sulfidation is complete. This sensor is the topic of U.S. Patent 9291543, "PC Board Mount Corrosion Sensitive Sensor," 2016.

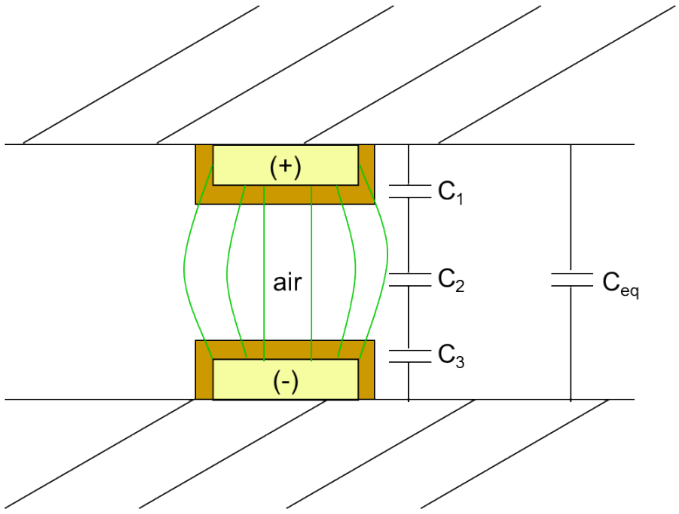

Figure 20. Improved capacitive sensor design.
Depiction shows partial conversion of copper to cuprous sulfide.

5. CONCLUSIONS

A great deal of progress has been made in developing readily deployable corrosion monitoring sensors. In the format of a solderable surface mount device, these sensors are small, light-weight, and capable of insertion very near points of concern. Sensitivity to corrosion can be tailored through thickness of metal deposition, and the resistance or capacitance ranges can be tailored through dimensions of length and width. Capacitive sensors can be designed as switches to dramatically change response after a threshold exposture to a corrosive environment. A new layout is designed to function with a continuously changing response. Sensors tested here were microfabricated by the hundreds (aluminum) and thousands (copper) using Sandia's microfabrication facilities. Further experimentation has taken place for government customers, leading to further characterization that is not reported here.

REFERENCES

1. Morten S. Jellesen, Vadimas Verdingovas, Helene Conseil, Kamila Piotrowska, Rajan Ambat, “Corrosion in electronics: Overview of failures and countermeasures,” Proceedings of EuroCorr 2014, 2014.
2. Harry Moffat, Amy Sun, David Enos, Lysle Serna, Rob Sorensen, and Corbett Battaile “Modeling Pore Corrosion in Normally Open Gold-Plated Copper Connectors,” SAND2008-5737, Sandia National Laboratories, Albuquerque, NM, 2008.
3. Nancy Missert, John P. Sullivan, David A. Czaplewski, David G. Enos, and R. Guild Copeland, “Advanced Sensors for Atmospheric Corrosion Detection,” SAND2006-0828A, Sandia National Laboratories, Albuquerque, NM, 2006.
4. Alex L Robinson, Kent B Pfeifer, Arthur N Rumpf, Anthony J. Ross III, Stephen W Howell, Neil R Sorensen, Samuel J Lucero, Maarten de Boer, and Richard W Cernosek “Embedded Evaluation – Advanced Sensor Development” SAND2008-6812, 2008.
5. John P Sullivan, J Charles Barbour, Nancy A Missert, R Guild Copeland, Thomas M Mayer, Michael J Campin, “The Effects of Varying Humidity on Copper Sulfide Film Formation,” SAND2004-0670, Sandia National Laboratories, Albuquerque, NM, 2004.
6. J C Barbour, J P Sullivan, M J Campin, A F Wright, N A Missert, J W Braithwaite, K R Zavadil, N R Sorensen, S J Lucero, W G Breiland, H K Moffat, “Mechanisms of Atmospheric Copper Sulfidation and Evaluation of Parallel Experimentation Techniques,” SAND2002-0699, Sandia National Laboratories, Albuquerque, NM, 2002.
7. Microchip Technology Inc. 2355 W. Chandler Blvd. Chandler, AZ 85224 USA.
8. CCS, Inc. Custom Computer Services, Inc. PO Box 2452 Brookfield, WI 53008.
9. Honeywell Sensing and Control,1985 Douglas Drive North, Golden Valley, MN 55422.
10. Analog Devices, Inc., Corporate Headquarters, 3 Technology Way, Norwood, MA 02062.

APPENDIX A. SENSOR PROCESS FLOW

Copper sensors were made using 0.025" thick ADS-996 amorphous alumina substrates from CoorsTek, Inc. (Golden, CO). The alumina wafers arrived as 4.5" x 4.5" squares, which were then cut with a CO_2 laser into 4" diameter rounds with an alignment flat for use in photolithography instruments. An oxygen plasma clean was performed using 600 sccm oxygen flow, 900 mTorr pressure, and 600 W power for 15 minutes. Three optical photolithography steps were then used to define the various metal layers and patterns, as depicted in Figure 21.

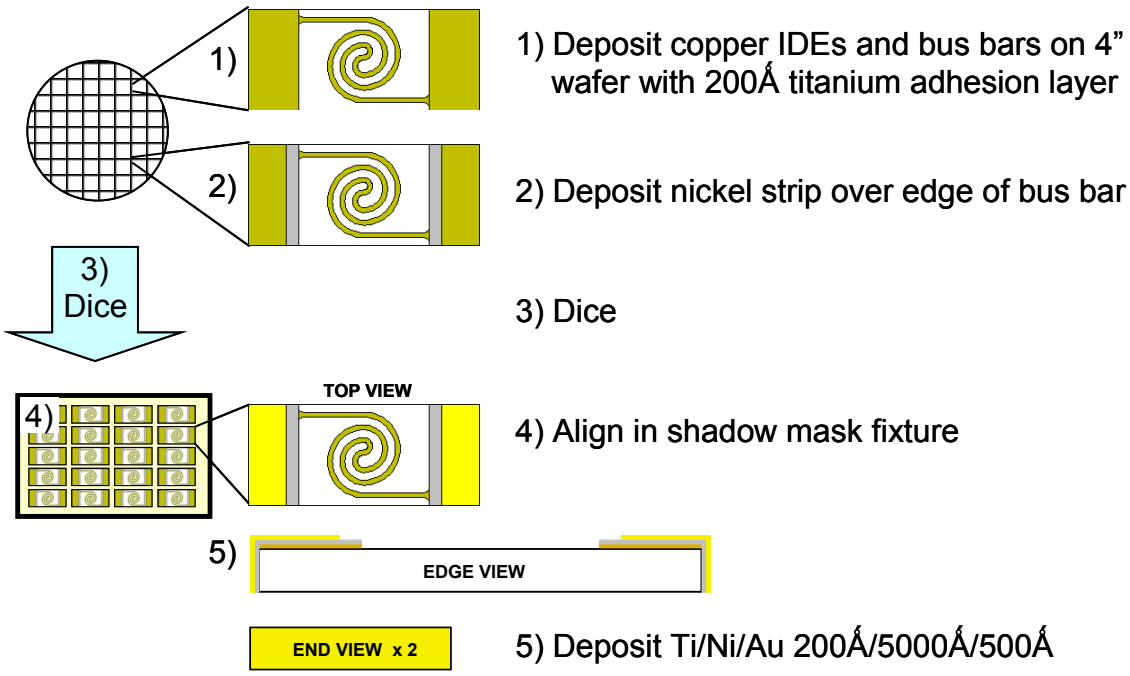

Figure 21. Numerous steps in-between: clean, spin coat, expose, develop, sputter, rinse, repeat.

Mask 1 was used to deposit a titanium adhesion layer and the copper sensor layer. Photolithography consisted of the following steps:

1. Heat-soak wafer in an oven at 90 °C.
2. Spin-coat HMDS and AZ4110 photoresists onto wafer at 4000 RPM for 35 seconds.
3. Bake at 90 °C for 90 seconds to set photoresists.
4. Expose photoresists to broadband UV light through contact Mask 1 for 2.6 seconds.
5. Develop photoresist in AZ400K developer (1:4 dilution with water) for 35 seconds.
6. De-scum in plasma cleaner with 500 sccm nitrogen, 900 mTorr pressure, and 200 W power.
7. Using a metal evaporator (e.g. Temescal), deposit 200Å titanium. Without exposure to oxygen (air), immediately deposit copper to desired thickness (500-2000Å here, but could be thicker).
8. Soak in acetone 1-2 hours to lift off remaining photoresist, which is also coated with the metals deposited above.

Mask 2 was used to deposit a nickel solder dam, which prevents solder from flowing into the sensing area when sensors are soldered to a PC board. Photolithography consisted of the following steps:

1. Heat-soak wafer in an oven at 90 °C.
2. Spin-coat HMDS and AZ4110 photoresists onto wafer at 3000 RPM for 35 seconds.
3. Bake at 90 °C for 90 seconds to set photoresists.
4. Expose photoresists to broadband UV light through contact Mask 2 for 2.8 seconds.
5. Develop photoresist in AZ400K developer (1:4 dilution with water) for 50 seconds.
6. De-scum in plasma cleaner with 500 sccm nitrogen, 900 mTorr pressure, and 200 W power.
7. Dip wafer in 0.1 molar hydrochloric acid for 30 seconds to remove oxidized copper. This ensure good adhesion to the next metal.
8. Using e-beam evaporation, deposit 200Å titanium. Without exposure to oxygen (air), immediately deposit 1000Å of nickel.
9. Soak in acetone 1-2 hours to lift off remaining photoresist, which is also coated with the metals deposited above.

Mask 3 was used to define the location of the solder pads and to protect the sensing areas during subsequent processing steps. LOR is used to protect the sensors from "hard baking" that occurs with standard photoresists at the high temperature of the sputter chamber used during the third metallization step. The recipe below results in a robust 9-micron-thick coating. Photolithography consisted of the following steps:

1. Heat-soak wafer in an oven at 90 °C.
2. Spin-coat LOR 30A onto the wafer at 2000 RPM for 30 seconds.
3. Bake at 150 °C for 5 minutes to set first photoresist.
4. Spin-coat AZ4110 photoresists onto wafer at 3000 RPM for 35 seconds.
5. Bake at 90 °C for 90 seconds to set second photoresist.
6. Expose photoresists to broadband UV light through contact Mask 3 for 8 seconds.
7. Develop top, AZ4110 photoresist in AZ400K developer (1:4 dilution with water) for 6:00 minutes.
8. Develop bottom, LOR 30A photoresist in MIF 319 developer for 4:00 minutes.
9. De-scum in plasma cleaner with 500 sccm nitrogen, 900 mTorr pressure, and 200 W power.

After development of the third set of photoresists, the wafers were diced using an 0.008" wide diamond wafer saw to the dimensions of the sensor (2.0 x 2.6 mm). The wafer flat ensured alignment. Particulates were cleaned away using DI water. Afterwards, the singulated, in-process sensors were moved to Sandia's AMPL for deposition of the soldering pads. The third metallization consisted of 3 metals deposited in a sputtering chamber without exposure to air between steps. After an argon plasma to remove copper oxides, the following layers were sputtered on the sensors through a shadow mask: 1000 Å titanium/50,000 Å Nickel/5000 Å gold. The shadow mask protects the photoresist-covered sensor area from the relatively thick metallization while allowing the solder pad materials to deposit on the top and end sides of the sensor to form the solder pads. This process is followed by removal of hard-baked photoresist on top of still-soluble LOR 30A using the LOR developer bath. After a final clean, sensors are stored in a dry nitrogen environment until ready for use.

Aluminum corrosion sensors (serpentine and IDE) were made by similar methods, using sapphire substrates. The same masks and processing steps were used, except that aluminum was deposited (with 0-3.5% copper) using e-beam evaporation.

APPENDIX B. DETAILED PC BOARD DESCRIPTIONS

Resistor Board. Figure 22 is the schematic diagram of the resistance PC test board. On-board programming and power is supplied via J2 according to Microchip and CCS documentation, and the details are not repeated here except to note that the microcontroller is configured to mimic a UART. This allows communication via any program that supports serial communication via J1 [7,8]. Programs such as *HyperTerminal*, *LabVIEW*, and Agilent *VEE* have been used to communicate with the system.

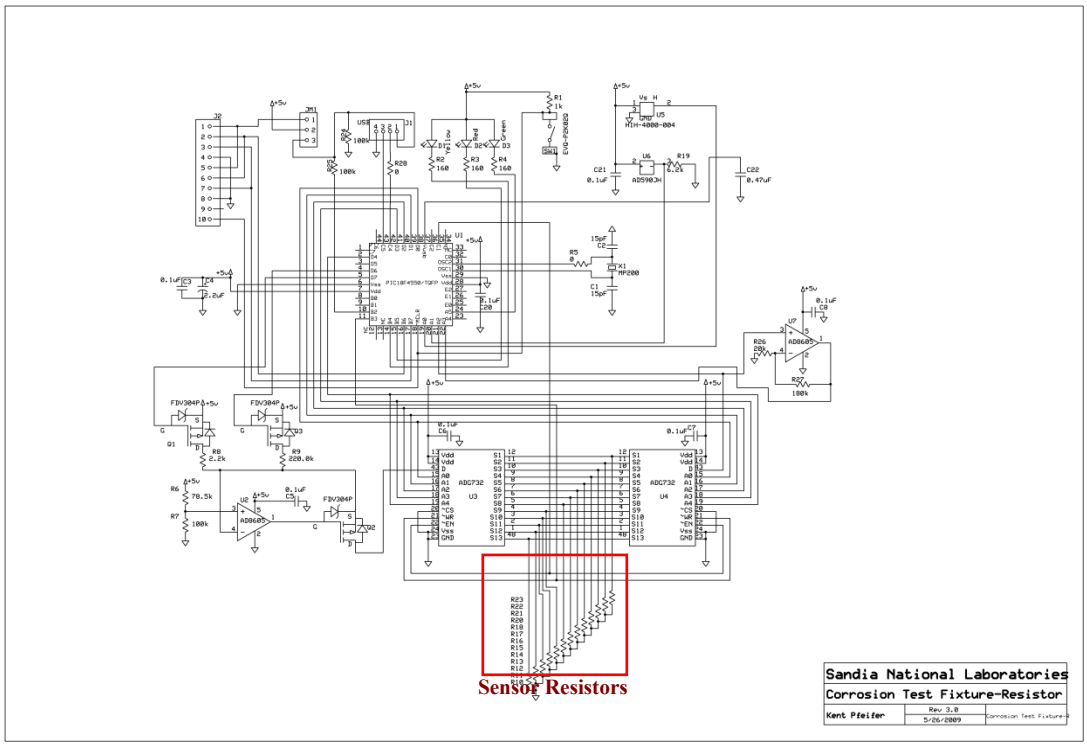

Figure 22. Schematic diagram of corrosion board for resistance measurement illustrating the microcontroller and measurement sections.

The firmware in the microcontroller was setup to operate in a software handshaking mode, where the main program first requests a measurement to be made and then waits for the system to make the measurement and send the response back to the main program. This allows precise control over the board but reduces the measurement speed for the application. Since these boards are intended to monitor a chemically slow process, this reduction in speed is not significant for this application.

Monitoring of the resistance structures was accomplished by first constructing a constant current source around an AD8605 single sided operational amplifier (U2). In the circuit of U2, a MOSFET is used to inject a constant current into the feedback loop of the amplifier. Two currents could be selectively injected, 1 mA via Q1 and 10 µA via Q3. This was controlled via firmware from the microcontroller. When a particular current was selected by raising the potential on the gate of the MOSFET to logic 1 (5 V), the MOSFET turned on and current began to flow through the feedback loop, causing the AD8605 to turn on Q2. Since the current into the AD8605 at the negative terminal was essentially zero, all of the current from Q1, and Q3 flowed through Q2 and into the multiplexer U3 (ADG732).

U3 and U4 were each 5-bit multiplexers operated in parallel such that they both switched to the same channel synchronously. Thus, current was directed to an individual resistor, and the potential produced across that resistor was switched to the 10-bit A/D on the PIC 18F4550 for measurement. The measurement sequence proceeded as follows. First, the smallest current (10 μA) was selected by the microcontroller, and the voltage on A2 and A3 of the microcontroller was measured. A2 was the direct measurement, and A3 was the voltage amplified using a non-inverting amplifier with a gain of 10 (R27/R26+1=10). The two measured values were stored. The current then increased to 1 mA, and the measurement was repeated. A software automatic ranging algorithm was implemented to check which value was the largest without driving the A/D to over-range. The resistance was calculated from the known current and gain. This allowed the system to measure voltages over 4 orders of magnitude without over-driving current on the sensors or other electronics. These voltage ranges were 0.010 mA*R_{test}, 0.10 mA*R_{test}, 1.0 mA*$R_{test,}$ and 10.0 mA*R_{test}. Thus, resistances as small as 0.5 Ω (assuming 1 bit of noise) to 500 kΩ could be measured. Figure 23 shows a plot of the resistance measured using the board compared to measurements with a Fluke 87 handheld ohm meter. The resistance board showed excellent linearity and accuracy.

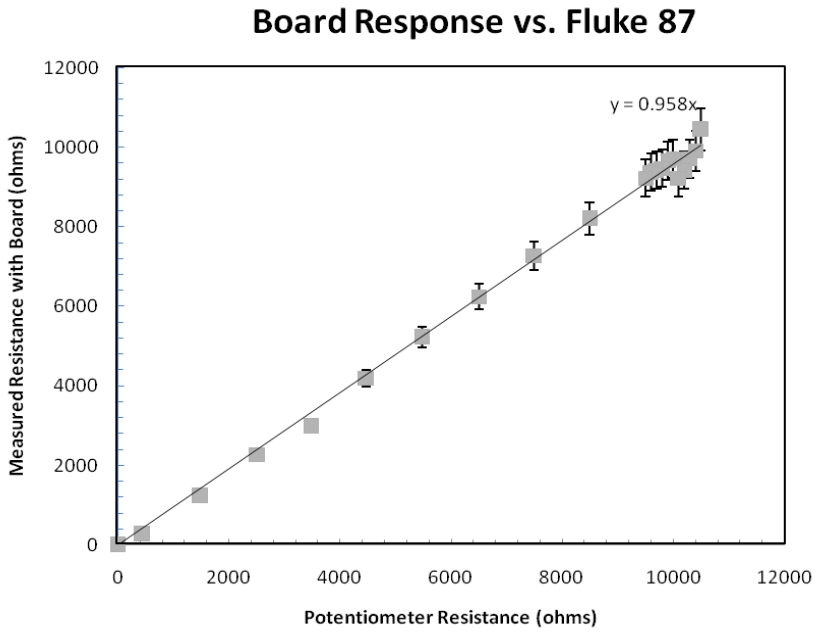

Figure 23. Plot of resistance measured using the hardware compared to a Fluke 87 digital ohm meter. Error bars are set to 5%.

The main commands for the board are given in Table 4. Measurements were made via USB from the control software using a single character. All of the commands could be displayed by typing "m" or "M" from the command line in ***HyperTerminal***.

Table 4. Table of Board Commands 1.

'R' or 'r'	Reads corrosion channels and returns the resistance value. Over range returns 999999.9Ω. Capital returns labels, lower case returns no labels.
'H' or 'h'	Returns temperature and humidity. Capital returns labels, lower case returns no labels.
"M" or "m"	Returns a complete listing of the commands for the system.

Capacitor Board. The capacitor board (Figure 24) functions similarly to the resistor board except for the measurement sections. The approach was to measure the time constant of the system and then deduce the capacitance via the following relationship:

$$C = \frac{t}{0.416R} \qquad \text{* MERGEFORMAT (1)}$$

Eq. * MERGEFORMAT (1) returns the capacitance of the system by measuring the interval between the beginning of a logic 1 pulse sent to an RC low-pass filter constructed from a fixed resistor and the capacitor-based sensor and the transition of the Schmitt triggers (U2 and U3). Referring to Figure 24, we see the 12 RC low-pass filters outlined by a box drawn on the schematic. Each of the filters is driven via a separate digital line from the microcontroller. The node between the capacitor and the resistor is connected to an inverting Schmitt trigger that makes a sharp transition between logic 1 and 0 when the voltage on the capacitor rises to 1.7 V. The Schmitt triggers return a logic 0 (0 V) output when the RC circuits on their inputs are at a non-charged condition. However, when a pulse was initiated by the microcontroller, the voltage on the capacitor began to rise as charge collected on the capacitor. When this voltage reached a nominal value of 1.7 V, the Schmitt trigger transitioned to a logic high condition, which forces the output of U4 (74F133 13-bit NAND) to transition from logic state 1 to 0. Thus, using the internal timers on the microcontroller and monitoring the output of the NAND gate, the number of clock cycles was counted during the elapsed time.

Eq. * MERGEFORMAT (1) was derived as follows from the transfer function of an RC network.

$$\frac{V(t)}{V_0} = 1 - e^{-t/RC} \qquad \text{* MERGEFORMAT (2)}$$

$$-\frac{t}{RC} = \ln\left(1 - \frac{V(t)}{V_0}\right) \qquad \text{* MERGEFORMAT (3)}$$

$$C = -\frac{t}{\ln\left(1 - \frac{V(t)}{V_0}\right)R} = \frac{t}{0.416\,\mathrm{R}} \qquad \text{* MERGEFORMAT (4)}$$

The values of R in the circuit were 2.2 MΩ, and the sensors had nominal starting capacitances of 15 pF, leading to an average time delay of about 13 microseconds. The clock on the microcontroller operated at approximately 6 MHz, implying that each count represented an elapsed time interval of 0.167 microseconds. Thus, the minimum resolvable capacitance change was calculated to be 0.200 pF. This was verified with the data of Figure 25, which shows a linear fit of a series of data points compared to the delay measured with an HP-54645D oscilloscope. In the experiment, a series of known capacitor values were installed on the board and the rise time

was measured until the Schmitt trigger transition was detected by the microcontroller. This data also shows excellent linearity.

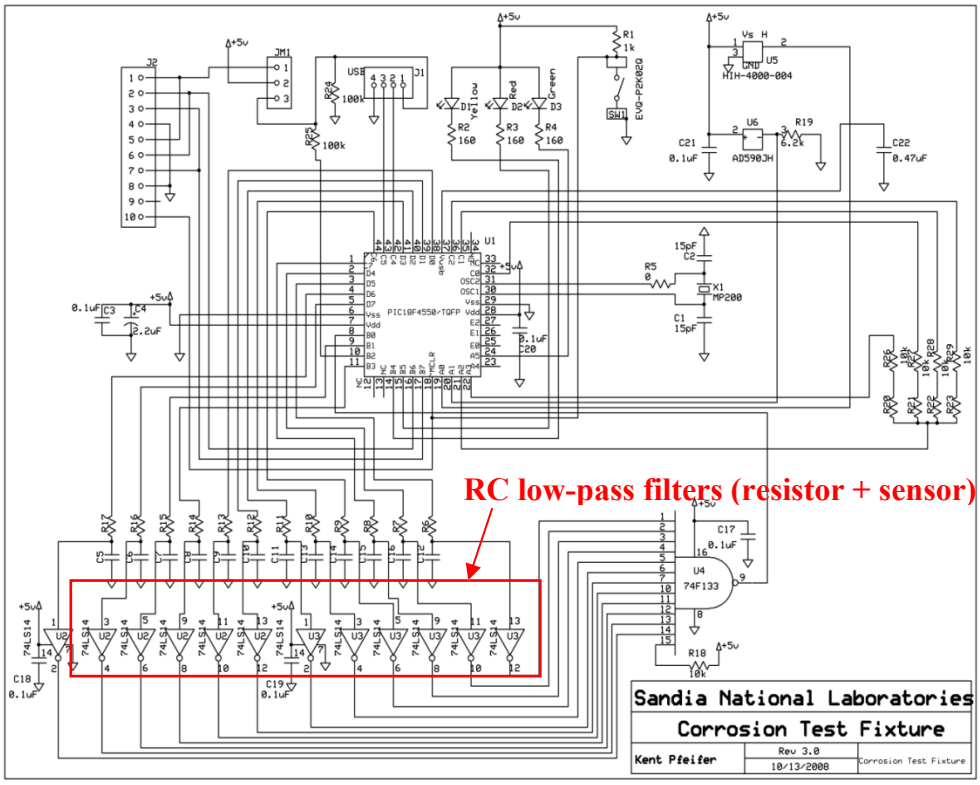

Figure 24. Schematic diagram of capacitance sensor measurement circuit.

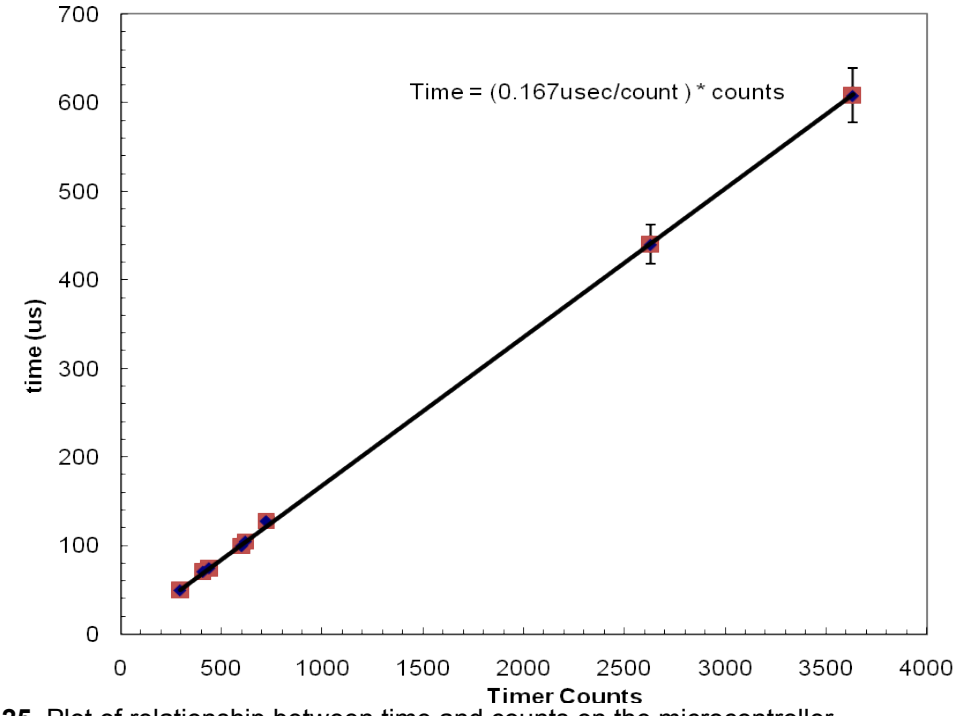

Figure 25. Plot of relationship between time and counts on the microcontroller. Linear fit of data indicates that each count represents 1.677 microseconds/count.

The firmware for the capacitance board is written in CCS PIC Micro MCU C [8]. The main commands are given in Table 5 and have the same format as for the resistance board.

Table 5. Table of Board Commands 2.

'C' or 'c'	Returns the number of counts from the timer representing the time constant. Capacitance is calculated from Eq. * MERGEFORMAT (1). A system return of value 0x1800 implies a "time-out" condition and indicates either a failure to trigger or a device failure.
'H' or 'h'	Returns temperature and humidity. Capital returns labels, lower case returns no labels.
"M" or "m"	Returns a complete listing of the commands for the system.

Environmental Sensors. Both PC boards were equipped with a Honeywell [9] HIH-4000-004 relative humidity sensor and an Analog Devices [10] AD590JH temperature sensor. Software was implemented to return values of the relative humidity and temperature from measurements of the output of these commercial sensors. In both cases, the "H" or "h" command returned the measured values. Per the data sheet, the temperature was calculated from a measured voltage by way of the following equation.

$$T(C) = \frac{V_{measured}}{10^{-6} A/K * 6200\Omega} - 273K \qquad \text{* MERGEFORMAT (5)}$$

For Eq. * MERGEFORMAT (5), the slope of the sensor current response from the AD-590 data sheet was used: 1 μA/K. Thus, Ohm's law implied that the current multiplied by the resistance value (6.2 kΩ) should return a voltage proportional to the temperature, which was then converted to Celsius as indicated above. The minimum resolvable temperature step was limited by the number of A/D bits (10) and was calculated to be 0.8ºC.

The humidity was calculated via the voltage measured at the output pin (2) of the HIH-4000 sensor per the following equation

$$RH(\%) = \frac{V_{measured} - 0.958\text{V}}{0.03068\,{}^{V}/_{RH}} \qquad \text{* MERGEFORMAT (6)}$$

where 0.958 V was the nominal offset in the voltage, and 0.03068 V/RH was the slope of the response to percent humidity. The minimum resolvable humidity change was calculated to be 0.2% RH.

DISTRIBUTION

1	MS0114	David V. Wick	1932 (electronic copy)
1	MS0346	Diane E. Peebles	1556 (electronic copy)
1	MS0353	Gerald M. Boyd	5355 (electronic copy)
1	MS0524	Robert W. Boney	2632 (electronic copy)
1	MS0525	Alex L. Robinson	2632 (electronic copy)
1	MS0889	Neil R. Sorensen	1852 (electronic copy)
1	MS0892	Stephen W. Howell	1765 (electronic copy)
1	MS0959	Adrian L. Casias	1833 (electronic copy)
1	MS1415	Nancy A. Missert	1124 (electronic copy)
1	MS1425	Kent B. Pfeifer	8634 (electronic copy)
1	MS156	Shawn M. Dirk	2241 (electronic copy)
1	MS0899	Technical Library	9536 (electronic copy)


Sandia National Laboratories